

Sol-gel matrices for controlled release: from macro to nano using emulsion polymerisation

Christophe J. Barbé · Linggen Kong · Kim S. Finnie · Sandrine Calleja ·
John V. Hanna · Elizabeth Drabarek · David T. Cassidy · Mark G. Blackford

Received: 4 October 2007 / Accepted: 29 February 2008
© Springer Science+Business Media, LLC 2008

Abstract By combining sol-gel technology with emulsion chemistry, it is possible to produce spherical particles with a designed microstructure based on a judicious choice of solvent/surfactant and sol-gel reaction parameters. When an active molecule is located in the aqueous droplet of a water-in-oil (W/O) emulsion, encapsulation occurs as the silicon precursors polymerise to build an oxide cage around the active species. By changing the solvent-surfactant combination, the particle size can be varied from 10 nm to 100 μm . The size of the particles is controlled by the size of the emulsion droplet, which acts as a nano-reactor for the sol-gel reaction. The release profiles can be tailored, independently of the particle size, by controlling the internal structure of the particles: pore volume, pore size, tortuosity, and surface chemistry (e.g. by introduction of trialkoxysilane). This can be easily achieved by controlling sol-gel processing parameters such as the water-to-alkoxide ratio, pH, alkoxide concentration, ageing, drying time and temperature.

Keywords Controlled release · Drug delivery · Nanoparticles · Micro-particles · Micro-encapsulation · Encapsulation · Sol-gel

Electronic supplementary material The online version of this article (doi:10.1007/s10971-008-1721-4) contains supplementary material, which is available to authorized users.

C. J. Barbé (✉) · L. Kong · K. S. Finnie
Ceramisphere Pty Ltd, Menai, NSW 2234, Australia
e-mail: chris.barbe@ceramisphere.com.au

S. Calleja · J. V. Hanna · E. Drabarek · D. T. Cassidy ·
M. G. Blackford
Institute of Materials Engineering, Australian Nuclear Science
and Technology Organisation, Menai, NSW 2234, Australia

1 Introduction

Controlled release technologies are gradually becoming an integral part of our everyday-life. With incorporation in products such as antiperspirant, herbicides, painkillers, battery tester, lipstick and razorblades, controlled release systems are present in an increasing number of industrial sectors. Although a wide range of organic compounds (such as natural gums, synthetic polymers, proteins, lipids and other surfactants) have been used to manufacture these capsules or particles, very few inorganic controlled release systems have found their way into industrial products. This is typically the case for ceramics which despite several intrinsic advantages such as their chemical resistance, their thermal and electrical stability as well as important biocompatibility and environmental-friendliness, remain an untapped resource for the manufacture of controlled release systems. This is mainly due to the high processing temperature employed in traditional methods of synthesis (typically $>1000^\circ\text{C}$), which is clearly incompatible with the encapsulation of organic molecules. The relative difficulty of manipulating the internal microstructure of the particles (as compared to polymers) also plays a role in their apparent lack of popularity as a controlled release matrix. However, both the high processing temperature and lack of control over the microstructure can be easily overcome using sol-gel technology, an ambient-temperature, inorganic polymerisation technique.

Since the early 1990s sol-gel technology has been used to encapsulate a wide range of molecules from dyes [1] or oils [2] to more complex biomolecules such as enzymes [3] and even biological entities such as bacteria [4] and whole cells [5]. The encapsulation is performed by simple addition of the molecules (or biological entities) during the formation of the oxide framework at ambient temperature

leading to the production of a composite gel with the active ingredient being homogeneously distributed throughout the resulting gel (or xerogel). Moreover, the physical characteristics (including density, pore size, and nanostructure) of the oxides produced by sol–gel processing can be tailored by controlling the sol–gel reaction kinetics, and in particular, the relative rates of hydrolysis and condensation [6]. This ability to control the xerogel microstructure is very important for the design of controlled release systems using sol–gel chemistry. For example, by switching from base to acid catalysis, the structure of the silica gel can be tuned from meso to microporous, consequently restricting the diffusion of the encapsulated molecules out of the sol–gel matrix and thus decreasing their release rate [7]. In a similar fashion, a wide range of processing parameters (water/alkoxide ratio, alcohol/alkoxide ratio, aging time, drying time and temperature, etc...) can be used to control the release rate by controlling the porous structure of the gel. This flexibility, and the extensive range of processing parameters available to control the release rate, has led to the manufacturing and testing of xerogels as sustained release implants and resorbable carriers to deliver a wide range of molecules, including antibiotics [8], anti-coagulants [9], analgesics [10], hypotensives [11], proteins [12], hormones [13], anti-oestrogen [14], anti-convulsants [15], anti-tumour agents [16] and even adenovirus [17].

Moreover, an increasing number of applications require the production of delivery systems in the particulate form such as micron size capsules containing flavours or essential oil for the food industry or polymeric nanoparticles for the treatment of cancers. In the case of sol–gel silica matrices, the question is how to produce particles with controllable size while preserving the control over the release offered by the sol–gel process. One answer lies in the fractionation of the sol–gel solution into micro-droplets, which will act as micro-reactors during gelation, thus producing silica particles with dimensions comparable to those of the micro-reactors. Two approaches have been used to achieve this: spray drying or emulsion polymerisation.

Although the successful production of controlled release microspheres was reported by Korteso et al. [18], spray-drying presents some significant limitations. The spray-dried particles are non-porous and the release is mediated by dissolution of the silica matrix. Only a limited control over the final release rate can be achieved as changes in chemical parameters lead to burst release and low production yield [19]. Spray-drying of less water soluble drugs (toremifene citrate or bisphosphonate [20]) leads to its segregation at the surface of the (hydrophilic) particles which results in an undesirable initial burst in the drug release profile. The size of particles produced by spray-drying is also limited to the micron range, thus precluding

applications requiring the production of nanoparticles, such as intravenous drug delivery. Finally, the intrinsic requirement of a relatively high temperature (i.e. $>120^{\circ}\text{C}$) during the drying step precludes the application of this method for the encapsulation of temperature sensitive biological molecules, such as enzymes or proteins.

To overcome these limitations and retain the close control over the release kinetics offered by sol–gel technology, we have developed an innovative method for producing micro- and nano-particles by combining sol–gel technology with water-in-oil (W/O) emulsions [21]. In the present paper it can be seen how the release rate and particle size can be precisely tailored by controlling the different processing parameters. For the sake of brevity only a few of the parameters influencing the release rate or particle size will be discussed and the focus will be on how the control over the release rate obtained in gels can be transferred to micro- and nano-particles.

2 Experimental

2.1 Chemicals

The surfactants sorbitan monooleate (Span 80), sorbitan monolaurate (Span 20), nonylphenoxypolyethoxyethanol (Triton N57 or NP-5: $\text{C}_9\text{H}_{19}\text{C}_6\text{H}_4(\text{OCH}_2\text{CH}_2)_5\text{OH}$), polyoxyethylene lauryl ether (Brij 30: $\text{C}_{12}\text{H}_{25}(\text{OCH}_2\text{CH}_2)_4\text{OH}$), polyoxyethylene isooctylphenyl ether (Triton X-114: $\text{C}_8\text{H}_{17}\text{C}_6\text{H}_4(\text{OCH}_2\text{CH}_2)_{7.5}\text{OH}$) and dioctyl sulfosuccinate (AOT) were purchased from Sigma Aldrich. Tergitol NP-9 ($\text{C}_9\text{H}_{19}\text{C}_6\text{H}_4(\text{OCH}_2\text{CH}_2)_9\text{OH}$) was purchased from Fluka. Methanol, chloroform, kerosene, hexane, decane, dodecane, cyclohexane tetramethyl orthosilicate (TMOS), tetraethyl orthosilicate (TEOS) and methyl trimethoxysilane (MTMS) were also purchased from Sigma Aldrich and used as received. Phosphate buffered saline solution (PBS) was prepared by dissolving one PBS tablet manufactured by Sigma in 200 ml of water yielding a 0.01 M phosphate buffer at $\text{pH} = 7.4$. Two dye molecules, Orange II (Sigma), and Rhodamine 6G (Sigma), were chosen as models because of their facile detection and quantitation by UV–vis spectrometry. Doxorubicin (Sigma) was chosen because of its extensively studied properties as an anti-cancer agent. Milli-Q water (resistivity $>18.3\text{ M}\Omega$) was used throughout.

2.2 General synthetic procedure

2.2.1 Monolith preparation

The procedure is summarised in Fig. 1. Typically, the different dye solutions were produced by dissolving

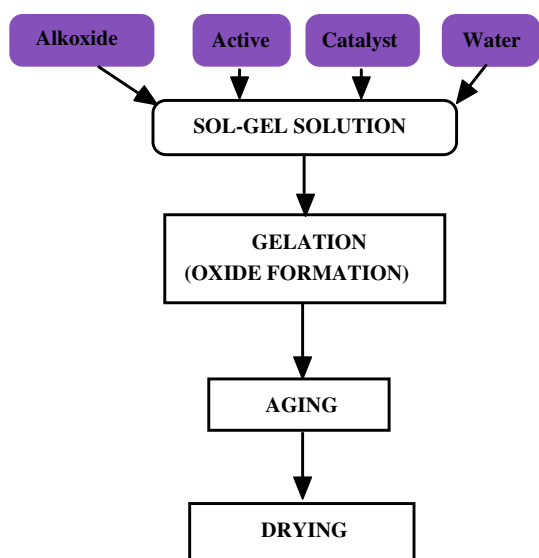


Fig. 1 Monolith synthesis flow-chart

0.100 g of Orange II dye in 100 ml of 0.1 mol/l nitric acid or 10 wt% aqueous ammonia and further adjusting, by titration, the pH to the desired value. The gel was synthesised by combining TMOS, methanol and the dye solution typically in a 1/4/4 molar ratio (TMOS:MeOH:H₂O). The resulting mixture was stirred for 1 h. About 4 ml aliquots of the solutions were transferred to 5 ml screw capped polypropylene vials and placed at 60°C in an oven to gel. Once gelation occurred, the samples were aged at 60°C for two more days. For each composition, one gel rod was set apart to study the release in the wet state and the remaining gel rods were dried at 60°C for 3 days. Note that different drying times and temperatures were used to study the influence of drying on the release.

2.2.2 Microparticle preparation

The experimental procedure for preparing the microspheres is summarised in Fig. 2. Typically, a sol-gel solution was prepared by combining TMOS, an aqueous solution of the active molecule at the desired pH, and methanol. The resulting solution was stirred for 30 min at 300 rpm and left to age for 1 day at ambient temperature. In parallel, a surfactant solution was prepared by dissolving a surfactant (e.g. Span 80 or Span 20) in a non-polar solvent (e.g. cyclohexane) followed by homogenization using a high-speed blender (8000 rpm for 60 s) to form a clear surfactant/solvent solution. The sol-gel solution was then added to the surfactant/solvent solution and the resulting emulsion was stirred at 500 rpm for 90 min. A suspension of microspheres formed, and was then filtered and washed 3 times with the solvent to remove the surfactant. The resulting microspheres were then dried at room temperature for 1 day, before further drying at 60°C for 3 days. The

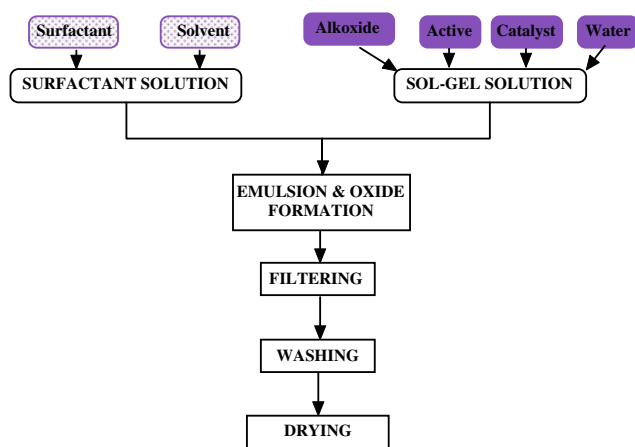


Fig. 2 Microparticles synthesis flow-chart

resulting powder was then stored in a sealed flask placed inside a desiccator.

2.2.3 Nanoparticle preparation

The experimental procedure for preparing nanoparticles is summarised in Fig. 3. Typically 7.560 g (12 mmol) of NP-9 was dissolved in 60 ml cyclohexane in a 250 ml screw capped container. About 1.304 ml (12 mmol) of 1-pentanol was added as a co-surfactant to provide enhanced stability to the emulsion. This mixture was shaken vigorously for about 1 min to prepare the surfactant solution. Then ammonia solution (1.33 mol/l NH₄OH: pH ~ 11.86, 1.296 ml) (72 mmol H₂O) containing the active molecules was added. The mixture was then stirred vigorously for about 30 min to produce a microemulsion. About 0.546 ml (2.4 mmol) of TEOS was added and the mixture was left to stir for 48–72 h at room temperature. This was followed by addition of 50 ml of dry acetone to destabilise the microemulsion. The system was further stirred vigorously for about 10 min. The silica particles usually flocculate and

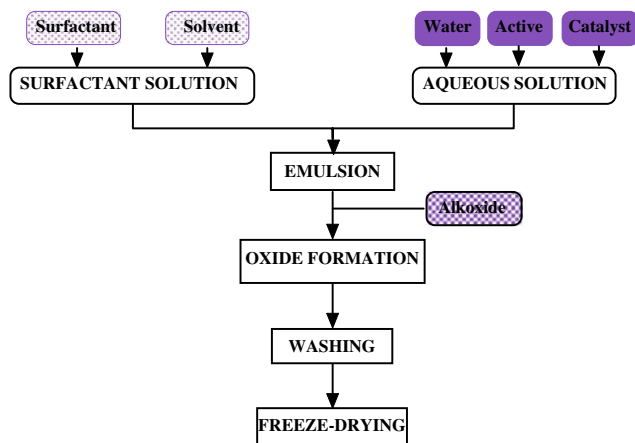


Fig. 3 Nanoparticles synthesis flow-chart

could be separated by decantation. If no significant sedimentation was observed, the mixture was centrifuged at 4000 rpm for 10 min. After sedimentation or centrifugation, the particles were separated from the organic phase and washed three times with 50 ml of dry acetone to remove the surfactant. After decantation of the acetone, 1.00 mol/l NaCl aqueous solution in the range of 20–50 ml (depending on SiO₂ mass) was mixed with the particles and transferred to a decantation funnel. The resulting suspension was washed 7 times using chloroform (50 ml) to further remove the residual surfactant, ultrasonicated and freeze dried using a Flexi-dry-84D freeze-drier (FTS Systems, Inc., Stone Ridge, NY).

Particles could also be synthesised with Triton X-114 and toluene. In this case 10.72 g (20 mmol) of Triton X-114 was dissolved in 100 ml of toluene. About 5.760 ml (320 mmol H₂O) of 1.33 mol/l ammonia solution was then added into the mixture and the resulting emulsion was homogenised by shear-mixing at 8000 rpm for 1 min. The emulsion was then stirred at 300 rpm and 0.304 ml (2 mmol) of TMOS was added. After 90 min, 50 ml of a 1.00 mol/l NaCl solution was added to the emulsion and the resulting suspension was transferred to a decantation funnel. After 12 h the emulsion was separated into two phases. The aqueous phase was extracted and 100 ml of toluene was added before re-introducing the mixture into a clean decantation funnel. This procedure was repeated several times, until the top organic phase became transparent. The final washed aqueous particle suspension was left to settle overnight. The supernatant was then removed to minimise the volume of liquid before freeze-drying.

2.3 Characterisation

The particle size and morphologies of the microparticles and nanoparticles were studied using a scanning electron microscope JEOL JSM6400 operating at 15 kV and a transmission electron microscope JEOL JEM 2000 FXII, respectively.

The porosity and surface area of the particles were characterised by nitrogen adsorption–desorption using an ASAP 2001 (Micromeritics). The corresponding data was treated using the classical BET and BJH approach as well as the more recent DFT (Diffusion Functional Theory) using software purchased from Micromeritics.

High-resolution solid-state ²⁹Si magic-angle-spinning (MAS) NMR spectra were acquired at ambient temperature using an MSL-400 NMR spectrometer ($B_0 = 9.4$ T) operating at the ²⁹Si frequency of 79.48 MHz. ²⁹Si MAS NMR data were acquired using a Bruker 7 mm double-air-bearing probe with cross-polarisation (CPMAS) and single pulse (Bloch decay) methods, both of which utilised high-power ¹H decoupling during data acquisition. The MAS

frequencies implemented for these measurements were ~5 kHz. For the ²⁹Si CPMAS experiments, a recycle delay of 5 s, a ¹H-²⁹Si Hartmann–Hahn contact period of 5 ms and an initial ¹H $\pi/2$ pulse width of 5 μ s were common to all CPMAS data. For the corresponding ²⁹Si MAS single pulse/high-power ¹H decoupling measurements, a single ²⁹Si $\pi/4$ pulse width of 2.5 μ s and a pre-acquisition delay of 10 μ s were used in conjunction with recycle delays of 30–60 s to ensure quantitative ²⁹Si measurements. All ²⁹Si MAS and CPMAS chemical shifts were externally referenced to tetramethylsilane (TMS) via a high purity sample of kaolinite, which was also used to establish the ¹H-²⁹Si Hartmann–Hahn condition.

The release rate of the dye molecules from the sol–gel matrix was characterised using UV–visible spectroscopy. The mechanism controlling the release of the active molecule from the sol–gel matrix is a combination of diffusion of the dye through the porous network and a gradual dissolution of the silica matrix. In this paper we concentrate on studying the influence of the processing parameters on the diffusion of the dye out of the matrix and thus have adjusted the sample to liquid ratio well above the 120 ppm solubility limit for the silica in aqueous media. The dissolution of the particles is studied elsewhere [22].

For the gel monoliths, the release of the dye from the gels was performed by typically introducing a sample of 0.15 g in 3 ml of water and monitoring the evolution of the absorbance with time at a fixed wavelength λ_{max} 485 nm (corresponding to the peak absorbance of Orange II) using a UV–visible spectrophotometer (Lambda 40, Perkin Elmer, USA). An experimental error of 5–10% was typically recorded for these measurements.

For the microparticles, the experiments were performed using an integrated automation package consisting of a VK7010 dissolution testing apparatus manufactured by Vankel coupled to a Cary 50 UV–vis spectrometer manufactured by Varian. This set-up allows for the simultaneous analysis of 7 samples under controlled temperature and stirring. The release studies were conducted by adding 0.5 g of particles in 100 ml PBS (pH = 7.4) at 37°C. Absorbance readings, at the wavelength corresponding to the peak absorbance of each dye, were recorded every 30 min for the duration of each release test. The quantity of dye released was then calculated using the Beer–Lambert law and the appropriate calibration curve. An experimental error of less than 2% was observed between samples synthesised under identical processing conditions.

The release of doxorubicin from nanoparticles was also monitored using UV visible spectroscopy. To investigate the doxorubicin release kinetics, 1 g of nanoparticles in sodium chloride (i.e. 0.15 g of nanoparticles) were re-suspended in 30 ml phosphate-buffered saline solution (PBS) (pH 7.4/25°C) in a polypropylene container, and

then centrifuged at 10,000 rpm for 1 h. The initial release was measured immediately. The sample container was then placed in a water bath at 37 ± 1 °C, with light rigorously excluded. At each time point, the particles were centrifuged (10,000 rpm \times 1 h), and the PBS supernatant was removed for analysis. Then fresh PBS solution was added and homogeneously mixed with nanoparticles with occasional agitation in the water bath. The release curve will show the accumulated release of the doxorubicin.

3 Results and discussion

3.1 Sol–gel monoliths (Macro)

3.1.1 Influence of the pH on the release rate

Orange II was encapsulated inside silica gel synthesized at different pH to study the influence of the pH on the dye release rate. Both acid and base are known [23] to catalyse the hydrolysis and condensation of silicon alkoxides. The rate of hydrolysis exhibits a minimum at pH 7, and increases exponentially at either lower or higher pH. In contrast, the rate of condensation exhibits a minimum at pH 2, and a maximum around pH 7. These effects can be used to control the size and shape of the inorganic polymers evolving in solution during sol–gel processing. At pH 2, extended, linear polymers are formed preferentially by end-chain condensation processes. In contrast, at higher pH, condensation occurs preferentially in the middle of the evolving oxopolymers, leading to extensive cross-linking and the formation of ramified, three-dimensional species. This trend is observed in the solid products as evidenced by ^{29}Si MAS NMR studies of the dried gel. The quantitative single pulse ^{29}Si MAS data of Fig. 4a exhibits a gradual increase of the proportion of Q4 fully condensed linkages (resonance at ~ -110 ppm) in comparison to populations of Q2 and Q3 species (resonances at ~ -92 ppm and ~ -102 ppm, respectively), with increasing pH. This observation corroborates the increase in structural condensation and cross-linking with increasing pH as reported by previous ^{29}Si solution NMR studies [23]. The spectral simulation and deconvolution of this data as shown in Fig. 4b demonstrate that this increase in Q4 linkages is promoted (almost) exclusively by further reaction of Q3 species, while the population of Q2 speciation remains unchanged throughout this pH range. A similar trend is observed by solid state Si NMR in the dried gel. Figure 4 reveals a gradual increase with pH of the proportion of Q4 and the corresponding Q2 and Q3 species. This confirms the increase in condensation and cross-linking with increasing pH as expected from the solution data available from the literature [23].

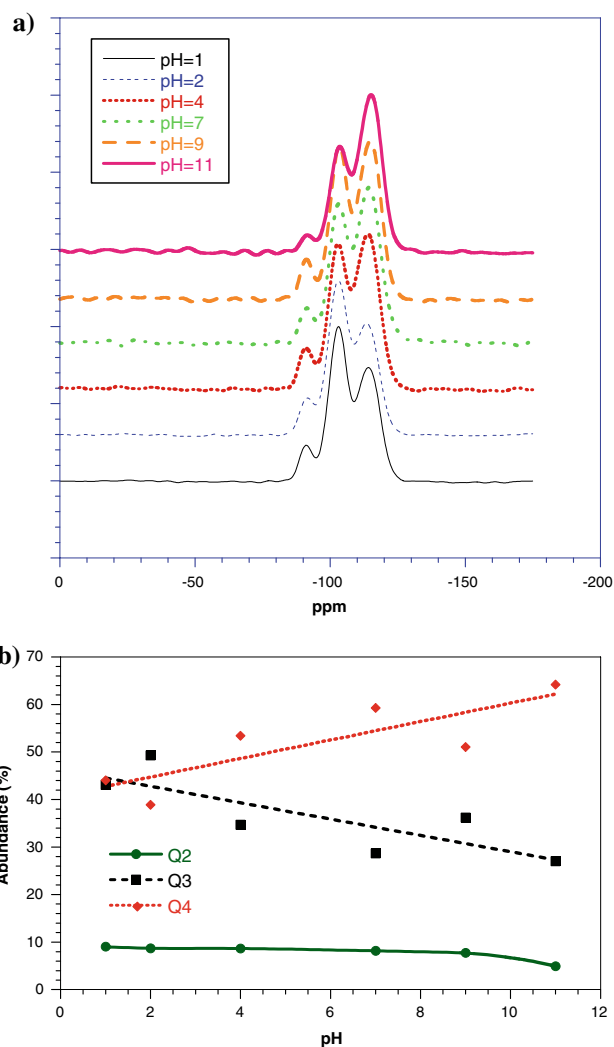


Fig. 4 Si MAS-NMR of gels synthesised at different pH (a) normal chemical shift spectra and (b) normalised Q population

Contrary to expectation, this increase with pH of density on the molecular level does not translate into an increase in the xerogel density. On the contrary, as can be seen from the nitrogen adsorption isotherms presented in Fig. 5, increasing the synthesis pH leads to the production of significantly more porous xerogels. This apparent contradiction can be explained by the contraction of the gel network during drying. The capillary pressure generated by the evaporation of the solvent from the “wet” lyogel exerts a considerable pressure (several MPa [23]), which leads to shrinkage (and sometimes shattering) of the monolith. Hydrolysis and condensation of the sol–gel solution at low pH (i.e. $\text{pH} \leq 2$) will lead to the formation of a tenuous and open framework that collapses on drying to yield microporous gels with a pore size centered around 1 nm (see Fig. 5b). As the pH increases, the cross-linking of the silicate polymer in solutions leads to stronger and denser alco-gel, which is more resistant to the capillary pressure

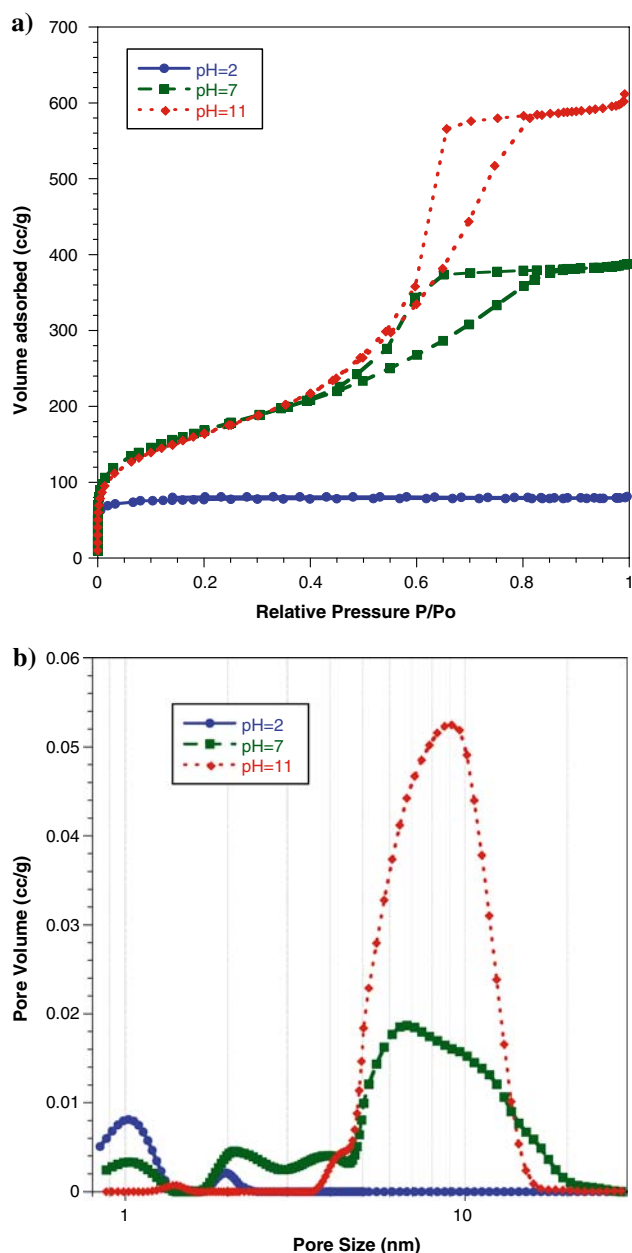


Fig. 5 Characterisation of gels synthesised at different pH using nitrogen adsorption (a) adsorption isotherms and (b) corresponding pore-size distributions calculated by DFT

generated during drying and thus leads to more open, less dense xerogel (see Fig. 5a). The strength of the silica network can be related to the degree of condensation of the silica, which, as can be seen from Fig. 4b increases with pH thus confirming the production of stiffer gel with increasing pH.

The DFT analysis of the nitrogen adsorption data (see Fig. 5b) reveals that the pore size distribution increases with pH. The gel produced at pH = 2 is purely microporous, exhibiting a type II isotherm with a corresponding pore size distribution centred around 1 nm. As the

synthesis pH is increased the pore size distribution shifts towards the mesoporous region and the gels exhibit type IV isotherms typical of mesoporous materials. At pH = 7, a broad pore size distribution is obtained spanning from 2 to 20 nm. When the pH is increased to 11, the distribution becomes narrower and is centred around 9 nm. The wide distribution obtained at pH = 7 corresponds well with the bushy tumbleweed structure described in the literature for neutral pH, where there exist a wide range of different size gaps between the silica framework. At pH = 11, the structure of the gel can be described in the term of a colloidal gel made by aggregation of fairly monodisperse silica spheres that aggregate together. This yields a more organised matrix with a smaller distribution of gaps between the silica networks than in the tumbleweed structure obtained at pH = 7. Thus one can see that by changing the pH of synthesis one can orient the microstructure of the gels from micro- to meso-porous solids.

It is therefore not surprising that the release rate was found to increase with increasing pH. Figure 6a shows that when the diffusion is restricted inside the micropores the release rate is extremely slow. As discussed above, as the pH increases, the pores become larger and the entrapped dye can diffuse faster out of the matrix. Although the final quantity of dye release does not increase with pH (e.g. quantity released at pH = 11 < quantity released at pH = 7), Fig. 6b shows clearly that the relative release rate (normalised to the maximum quantity released) does increase with increasing pH thus confirming that it is the pore size that controls the release rate of the encapsulated molecules. It is interesting to note that a similar trend was observed with a variety of other molecules with different functional groups and size [7].

3.1.2 Influence of the % of MTMS on the release rate

The substitution of TEOS or TMOS by MTMS introduces methyl groups into the silica matrix, changing the nature of the xerogel from a purely inorganic entity to a mixed organic–inorganic hybrid. The introduction of methyl moieties in the silica network can be observed in Fig. 7a by the emergence of additional downfield shifted resonances at ~ -56 ppm and ~ -64 ppm corresponding to the silicon T2 and T3 units, respectively, which are characteristic of more covalent Si–C bonds. The introduction of the methyl groups disrupts the cross-linking reaction by reducing the number of condensable Si sites and reducing the overall connectivity (or degree of condensation) of the silica network. As observed in Fig. 7b, the quantitative estimate of Q4 linkages decreases with increasing an MTMS/TMOS ratio thus lowering the overall structural connectivity. This decrease in the average degree of condensation leads to a decrease in the materials toughness and a corresponding increase in its ductility [24].

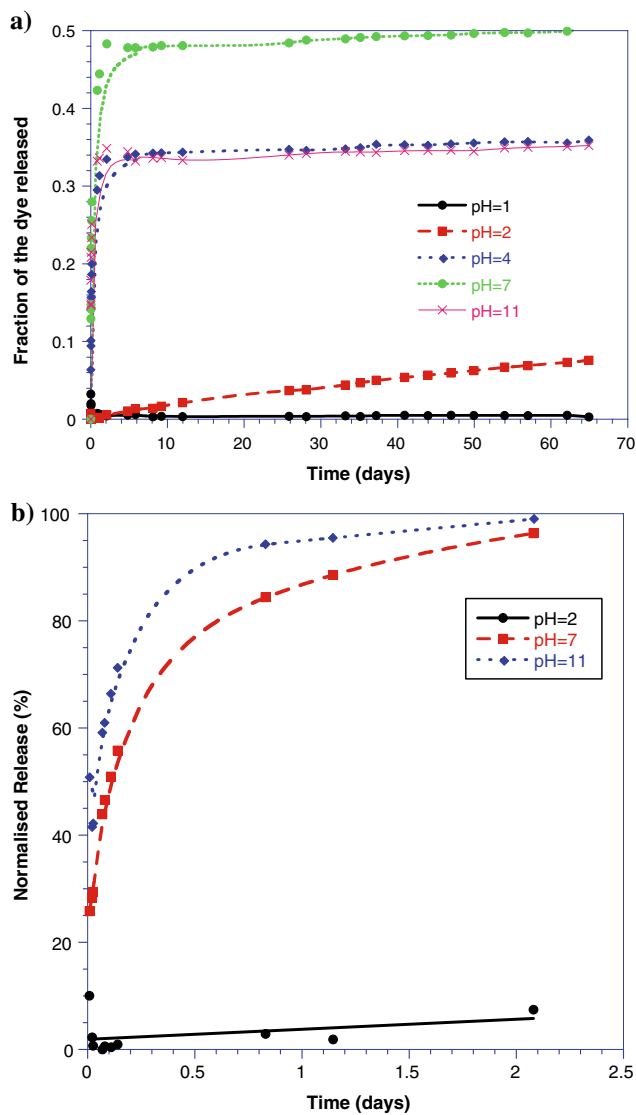


Fig. 6 Release curves of Orange II from gels synthesised at different pH

Accordingly one would expect, as discussed in the previous section, that a decrease in the silica network toughness would lead to a larger shrinkage under the influence of the capillary pressure during drying and thus would produce denser material. Figure 8 shows exactly the opposite, with the porous volume and average pore size increasing with increasing amount of MTMS introduced. This apparent contradiction can be explained by the ability of certain gels to spring-back and expand past the critical drying point [25]. This expansion can be expressed in the form of a volumetric strain given as:

$$e = P/K_p$$

where P is the capillary pressure and K_p the bulk modulus of the gel. As mentioned above the bulk modulus decreases with increasing amount of MTMS being introduced and

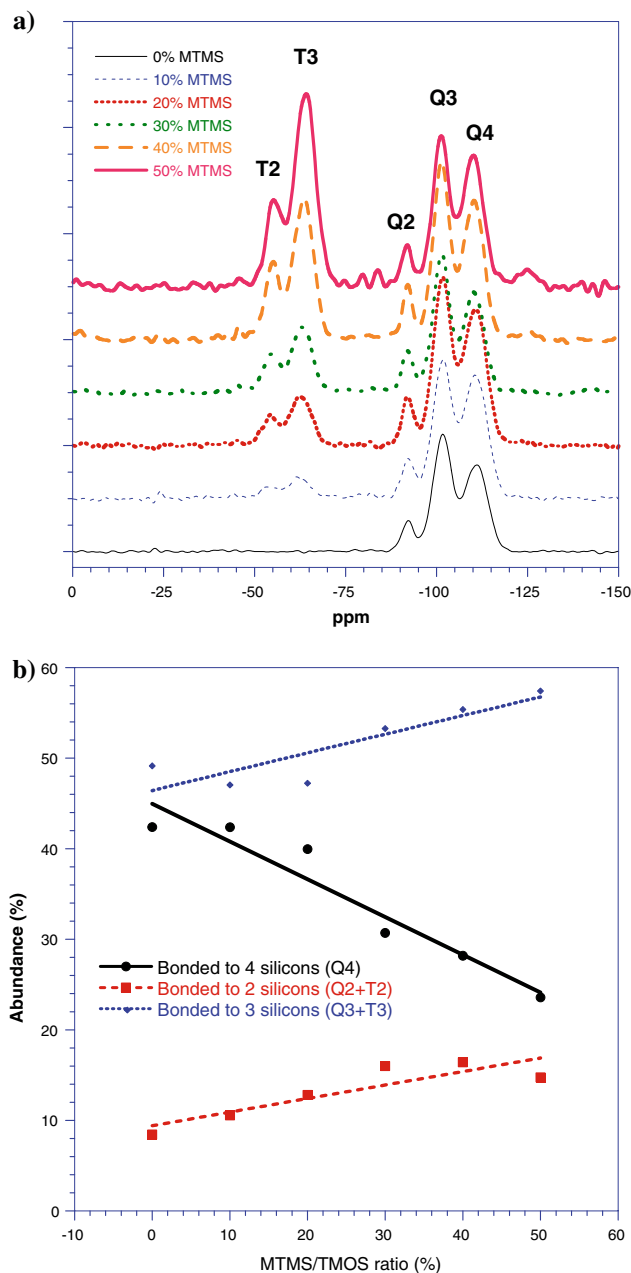


Fig. 7 Si MAS-NMR of gels synthesised with different amount of MTMS (a) normal chemical shift spectra and (b) evolution of the connectivity

thus decreasing the contraction of the gel upon drying. In other words, the incorporation of unreactive methyl groups in the silica network decreases the number of condensable sites in the gels. The decrease in reactive sites prevents the irreversible “zipping” of the pores when capillary pressure brings the two pore walls in contact and leads to the re-expansion of the gel past the critical drying point. The more MTMS introduced, the fewer anchoring points produced, resulting in more ‘springback’ and larger pore size in the dried gels.

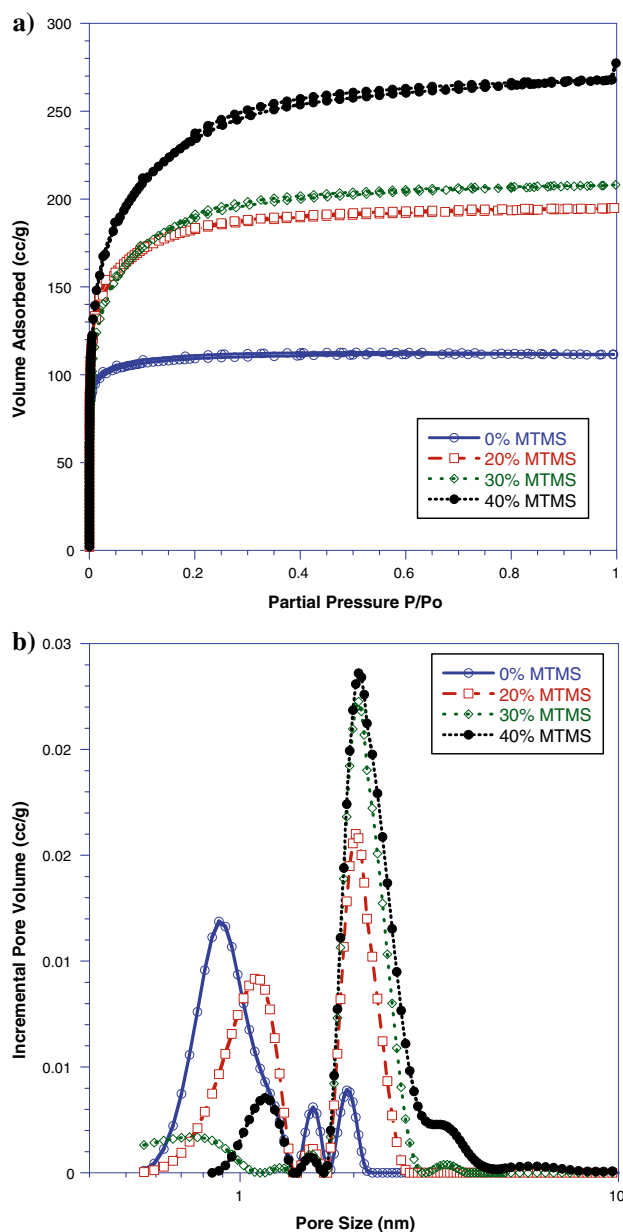


Fig. 8 Influence of the amount of MTMS on the porous structure; (a) Nitrogen adsorption isotherms and (b) corresponding pore-size distribution calculated by DFT

Surprisingly, the growth in pore size with increasing MTMS does not lead to faster release rates. On the contrary, the release rate decreases with increasing MTMS content (see Fig. 9). This apparent contradiction can be explained by the change in the nature of the gel with increasing amount of organically modified alkoxide introduced. The introduction of methyl groups in the silica increases the hydrophobicity of the matrix and thus gradually prevents the penetration of water into the pores of the gel, thus stopping the diffusion of the hydrophilic dye encapsulated inside.

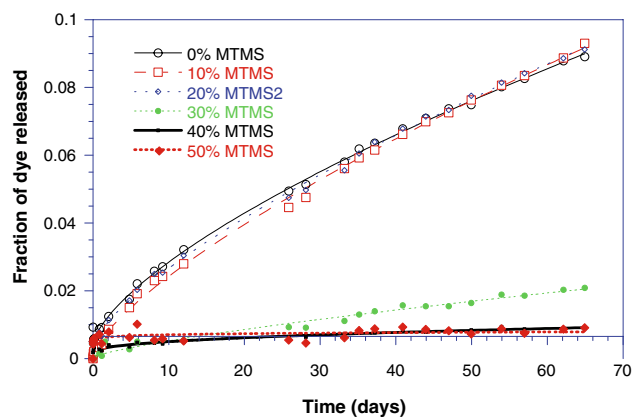


Fig. 9 Release of Orange 2 from gels synthesised with different amount of MTMS

3.1.3 Influence of the drying time and temperature

As we have seen in the previous paragraph most of the gel shrinkage takes place during the drying stage. It is therefore not surprising that drying temperature and time has a significant effect on the release rate. Increasing the drying temperature leads to an increase of the evaporation rate of the pore liquid and thus to an increase of the capillary pressure which will result in more shrinkage and the production of denser gel. This in turns leads to slower diffusion of the entrapped molecule out of the gels as can be seen from Fig. 10. A similar effect is observed for the

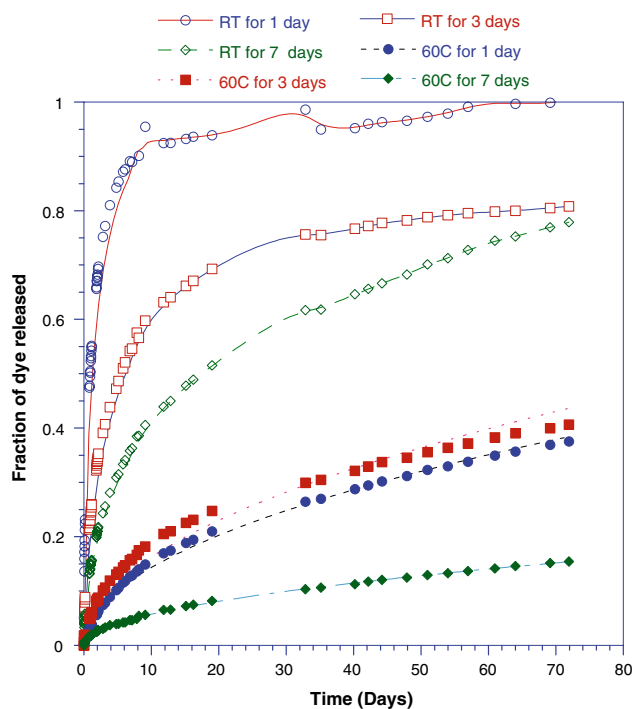


Fig. 10 Influence of the drying temperature and time on the release of Orange II from gel synthesized at pH = 2

drying time where increasing drying time leads to slower release rates. It is interesting to note that, although nitrogen adsorption measurements were attempted on gels dried at different temperature and time, no significant difference was recorded due to the averaging effect of the preconditioning drying at 80°C under vacuum required by the measurement protocol.

3.1.4 Conclusion

In summary, the release rate can be precisely tailored by controlling the internal microstructure of the xerogels. By controlling the pore size one can restrict the diffusion of the active molecules out of the gels. Denser microporous gels provide slow and extended release whereas mesoporous gels exhibit faster release. The introduction of organically modified silica can also decrease the release rate by changing the hydrophobicity of the matrix and thus slowing the penetration of water into the small pores.

4 Microparticles

As mentioned in the introduction, a number of applications require controlled release systems in particulate form. In our case, the challenge is how to control the particle size while retaining precise control over the release rate offered by sol-gel technology. The answer lies in compartmentalisation of the sol-gel solution into droplets of definite

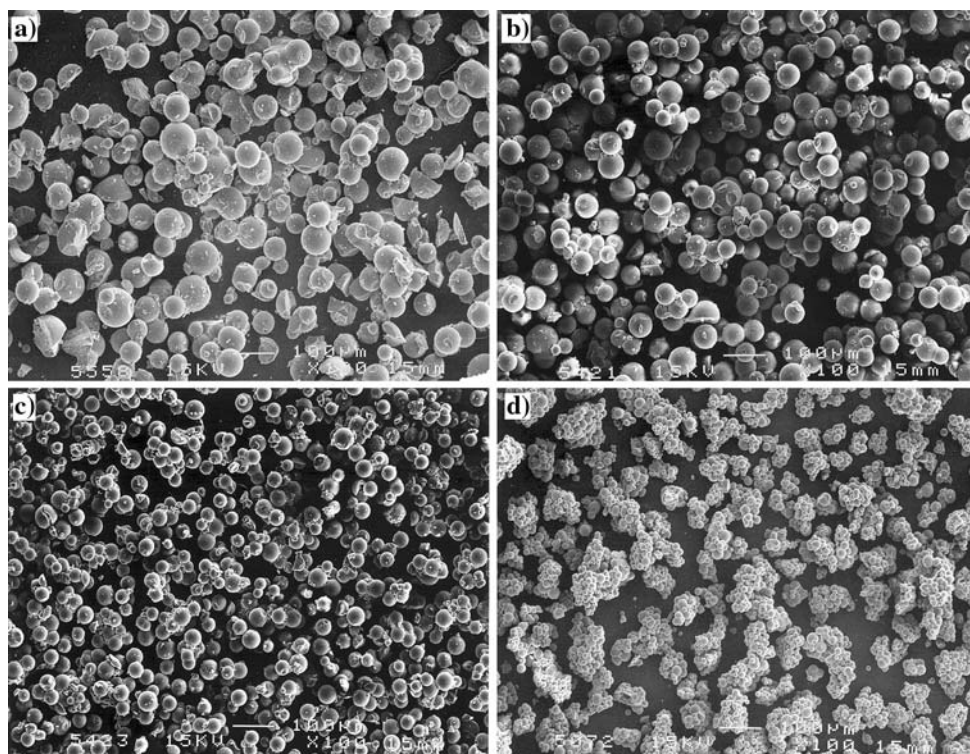
size. This can be achieved by emulsification of the sol-gel solution by mixing it with a solution composed of a surfactant and a non-polar solvent (see Fig. 11). Upon mixing, the polar sol-gel droplets are dispersed in the non-polar solvent and act as micro-reactors in which the gelation proceeds, yielding microparticles with size comparable to the droplets. Thus, one can control independently the particle size by controlling the droplet size through the emulsion parameters and the release rate by controlling the internal structure of the particles through the sol-gel processing parameters.

4.1 Control of the size

4.1.1 Influence of the solvent

Figure 11 shows that the particle size can be modulated by changing the non-polar solvent of the emulsion while keeping the other processing parameters constant. The surfactant used was sorbitan monooleate (Span 80). The particle size decreases with increasing chain length in the solvent, with even smaller particles obtained with cyclic hydrocarbons over straight alkanes. It is believed that a combination of increasing the dielectric constant and decreasing the interfacial tension will decrease the droplet size, but more importantly will reduce the coalescence of the droplets by stiffening the surfactant wall and thus preventing particles growth by aggregation [26].

Fig. 11 Influence of the emulsion solvent on the particle morphology: (a) hexane, (b) octane, (c) dodecane, (d) cyclohexane. Surfactant is Span 80. All scale bars: 100 μm



4.1.2 Influence of the surfactant

Figure 12 shows that the particle size can also be modulated by changing the surfactant while keeping the other processing parameters constant including the solvent which was cyclohexane. As mentioned above, the selection of the surfactant is critical in controlling the interfacial tension between the non-polar and polar phase and thus controlling the droplet size. More importantly, emulsions are dynamic

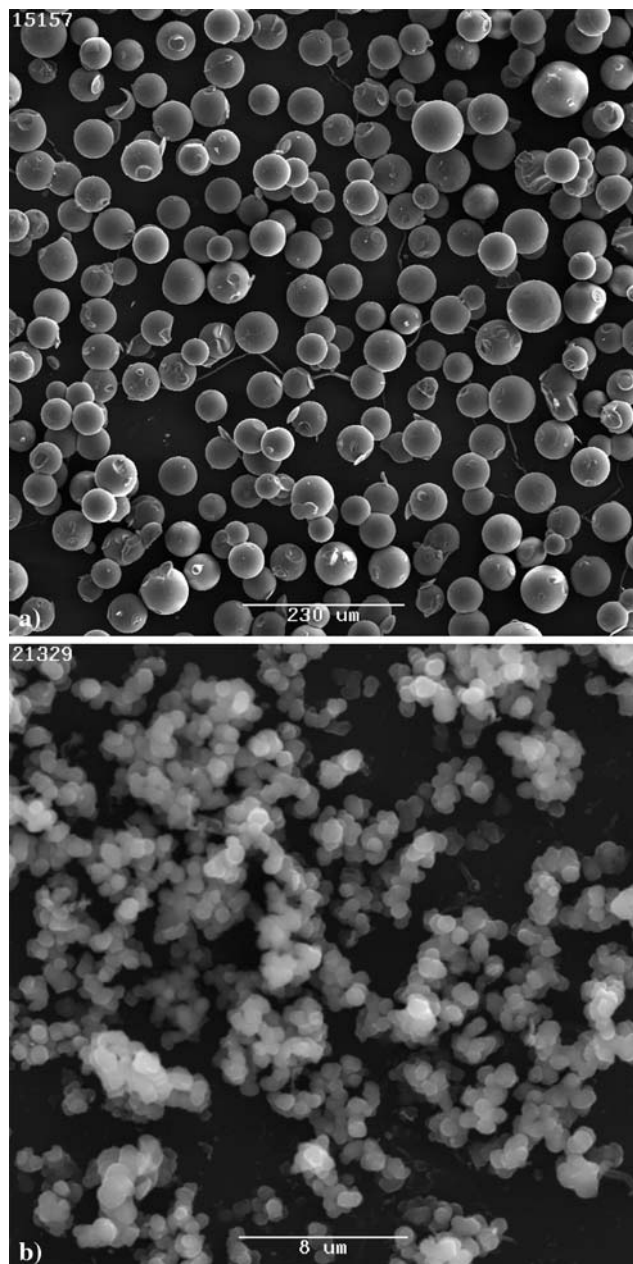


Fig. 12 Influence of the nature of the surfactant on the particle morphology. Particles synthesized with (a) span 80 in cyclohexane and (b) AOT in cyclohexane

systems where droplets constantly coalesce, exchanging their cores which induces particle growth by a coalescence/aggregation mechanism [27, 32]. Thus, the size of the particles can be controlled by either preventing or promoting coalescence of the droplets during their gelation inside the emulsion by careful selection of surfactant/solvent couple. Although no simple selection rule can be applied to predict which surfactant will give a particular particle size, it has been found that surfactant structure (e.g. longer head and tail group) can provide better stabilisation of the micelle walls and thus reduced inter-droplet exchange, resulting in the production of smaller particles [28]. In the particular example in Fig. 12, the two tails of AOT do provide a better stabilisation over the single hydrophobic alkyl tail of the sorbitan mono-oleate. AOT is in fact known as having one of the lowest inter-micelle exchange rates among typical micro-emulsion systems [29].

4.2 Control of the release rate

4.2.1 Influence of the pH

To assess whether the release rate of the encapsulant could be controlled by tailoring the internal structure of the sphere using different sol-gel parameters, different particles were synthesized by combining an identical surfactant solution with different sol-gel solutions synthesized at different pH (i.e. 2, 7 and 10). SEM analysis of the corresponding particles showed identical size distributions (data not shown).

N_2 adsorption-desorption analysis (see Fig. 13) shows clearly the influence of the pH on the internal structure of the spheres. The sample synthesized in base exhibits a typical mesoporous isotherm as the one synthesized in acid exhibits a stronger microporous component. This difference is further reflected in the pore size distribution which clearly shows a significant increase in the pore size distribution from acid to base. This confirms that sol-gel chemistry does control the internal structure of gel produced inside emulsion droplets, in a similar way to bulk gel monoliths.

Moreover, this ability to control the internal structure of the microspheres allows the control of the release rate. As observed for the xerogels (see Fig. 6), the release rate of Orange II increases with the pH at which the microspheres have been synthesized. This faster diffusion for particles synthesized in base corresponds well with the increase in pore size with the pH of the sol-gel solution. The release of Rhodamine 6G exhibits the same trend although with smaller quantities being released over 48 h. This can be attributed to the large molecular size of Rhodamine 6G (MW: 479.02 positively charged) compared to Orange II

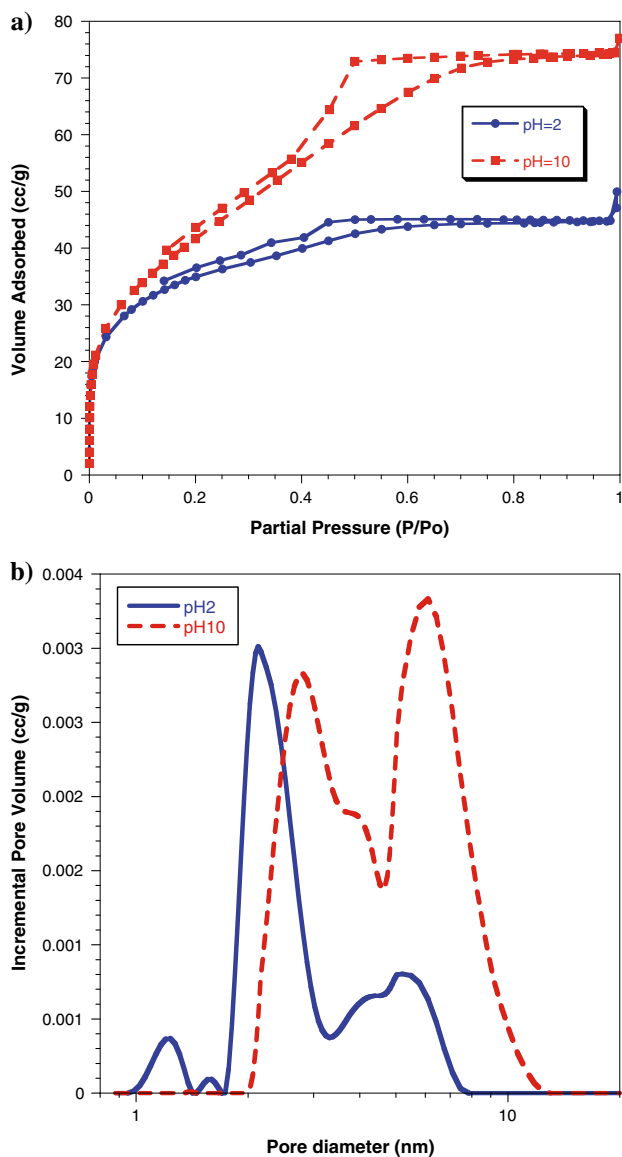


Fig. 13 Influence of the synthesis pH on the porosity of the microparticles: **(a)** nitrogen adsorption isotherms and **(b)** corresponding pore-size distribution calculated by DFT

(MW: 350.30, negatively charged) as well as the presence of amine groups that can have relatively strong affinity with the negatively charged surface of silica, thus slowing the diffusion of the molecule through the tortuous pore network. More importantly, the fact that the same trend (i.e. increase of the release with increasing synthesis pH) is observed for both molecules confirms that the release rate of the encapsulated molecules can be tailored by controlling the internal structure of the microspheres through sol-gel chemistry (Fig. 14).

Furthermore, the fact that the trends observed in the microspheres are identical to those observed for the xerogels demonstrates the validity of the micro-reactor analogy.

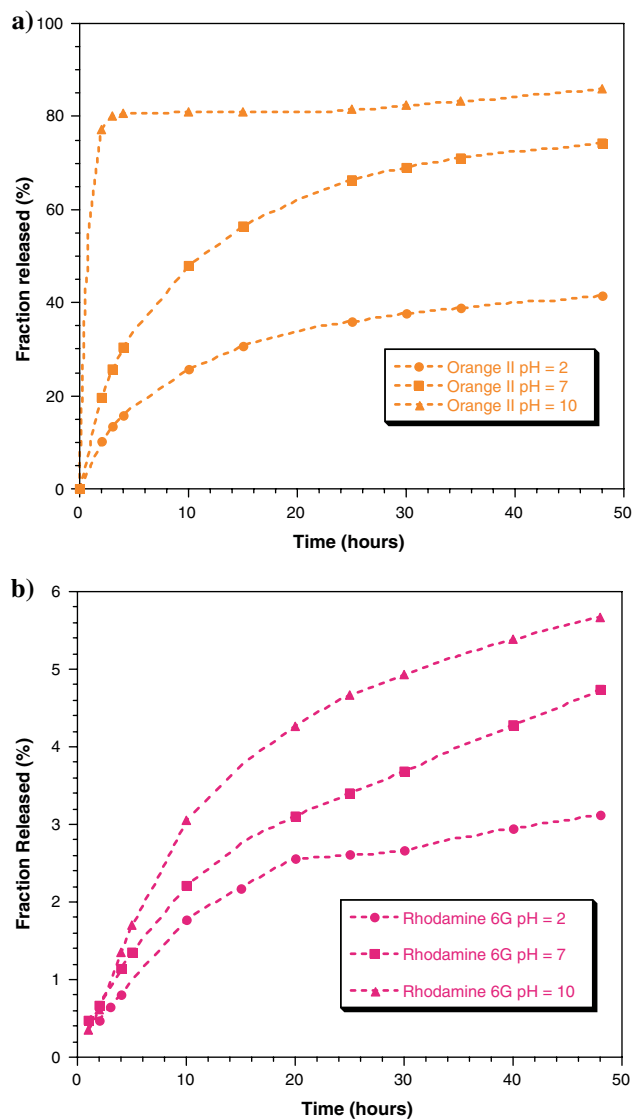


Fig. 14 Influence of the synthesis pH on the release rate of **(a)** Orange II and **(b)** Rhodamine 6G from microparticles

The difference in the release time scale between the particles and the gels (i.e. hours for the microparticles versus days for the gels) can be explained by both the difference in the release temperature (37°C for the microparticles versus 22°C for the xerogels) and the difference in average diffusion length (15 μm for the microparticles versus a few mm for the gels). The increase in temperature as well as the shorter diffusion path will accelerate dramatically (i.e. several order of magnitudes) the release rate of the encapsulated molecules. Moreover, even if the specific surface area of the microspheres and monoliths synthesised under similar conditions are similar, the proportion of active in contact with the external media (e.g. water) is very different in both cases. Indeed, at time 0, when the pores are filled with active, diffusion front corresponds to the geometrical surface area of the two objects. One can

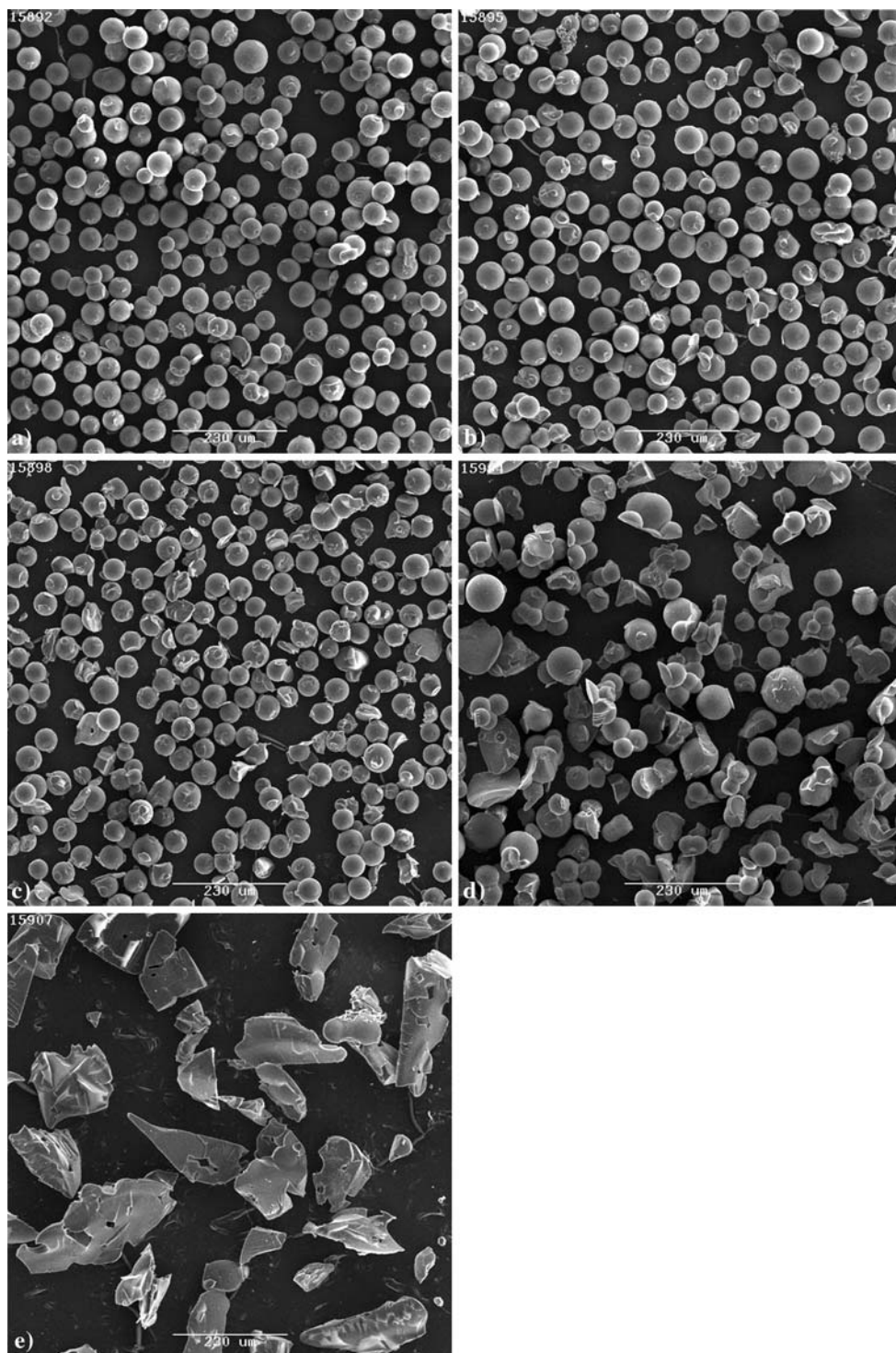
therefore see that for a similar internal structure, the smaller spheres will release faster than the larger monolith.

4.2.2 Influence of the % of MTMS on the release rate

The substitution of TMOS by MTMS in the sol-gel solution does not lead to significant change in the particle

morphology up to 15 mol%. At 20 mol% of MTMS the average particle size increases significantly, as well as the number of fracture fragments resulting from drying of very large particles. The particles are also significantly more aggregated (presence of fused particles with visible inter-particle necks). This fusion of the microspheres is dramatically accentuated for 25 mol% MTMS substitution,

Fig. 15 Influence of the molar fraction of MTMS on the microparticles morphology; SEM of micro-particles produced with (a) 0%, (b) 5%, (c) 15%, (d) 20%, and (e) 25% MTMS substitution. Scale bars: 230 μm



where most of the sample consists of gel fragments with a few fused particles still visible. This suggests that introduction of a large quantity of MTMS in the sol–gel solution destabilises the emulsions and leads to aggregation of the polar droplets into larger gel fragments. This increasing instability with MTMS content could be further explained by the increasing hydrophobicity (or lipophilicity) of the hybrid polymer by introduction of methyl groups in the silica network. This increase in hydrophobicity results in the potential migration of the hybrid silica polymer from the polar micellar core (i.e. polar droplet) to the outer non-polar phase and their resulting aggregation. In other words, the introduction of a large amount of organically modified silicon alkoxide leads to the destruction of the micro-reactors and the agglomeration of their contents (Fig. 15).

Nonetheless, the release rate can be gradually decreased by substituting an increasing amount of MTMS in the sol–gel solution (see Fig. 16). As observed in the xerogels, this gradual decrease in release rate can be explained by the increasing hydrophobicity of the pore surface which slows both the diffusion of water in and the diffusion of the hydrophilic dyes out.

4.2.3 Influence of the drying time and temperature

To study the influence of the drying on the release rate, a sample was synthesized under standard conditions (pH = 2, Si/H₂O/MeOH = 1/4/4) and dried for 40 h at room temperature and then further dried at different temperature and time. Surprisingly, SEM analysis did not reveal significant differences in the particle size distribution after drying at different temperature or time. This

could be explained by the fact that most of the shrinkage and consolidation of the silica network has been performed during the 40 h room temperature drying step. The importance of the room temperature drying on the densification of the particles is further exemplified by the shattering of the particles when the particles are immediately heated above ambient, thus bypassing this step.

Increasing both the drying time and temperature slows the release rate (see Fig. 17). As observed for xerogels, increasing the drying temperature and time lead to an internal densification of the sol–gel matrix, which

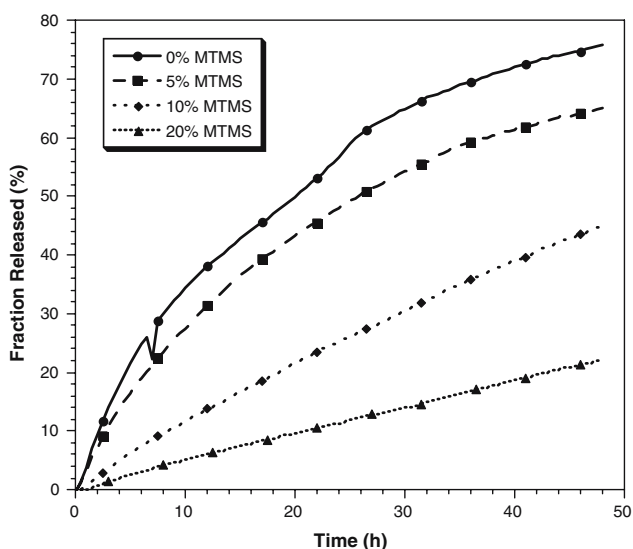


Fig. 16 Influence of the molar fraction of MTMS on the microparticles release rates

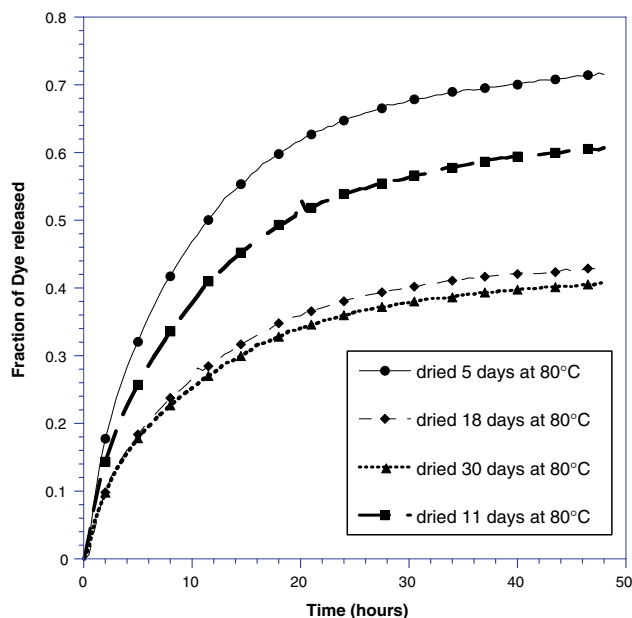
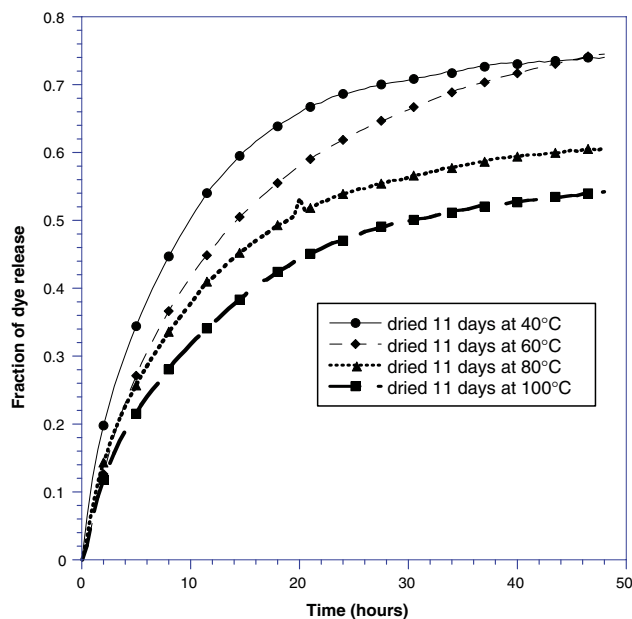


Fig. 17 Influence of (a) the drying temperature and (b) drying time on the release of Orange II from microparticles synthesized at pH = 2

decreases the pore diameter. Diffusion of the encapsulated molecules out of the silica spheres is thus restricted, decreasing the overall release rate.

4.3 Conclusions

Active molecules can be easily encapsulated inside silica microspheres by performing sol–gel polymerisation inside a “water”-in-oil emulsion. The particle size can be tailored by controlling the emulsion parameters such as the nature of the solvent and surfactant. The release rate is controlled by sol–gel processing parameters such as the synthesis pH, the extent of substitution with MTMS, and the drying time and temperature. More generally, the trends in release rate observed in the xerogels are preserved in the microparticles confirming the validity of the micro-reactor approach, which allows for independent control of the size and internal structure of the sphere. Moreover, the efficient compartmentalization obtained in an O/W emulsion, enables sol–gel reactions to proceed almost unaltered on the micron-scale.

5 Nanoparticles

5.1 Introduction

Certain applications such as intravenous drug delivery, and more specifically, passive targeting of cancerous tumours, require the production of nanoparticles which are stable in the blood stream. Hydrodynamic stability in the blood stream is achieved by keeping the particle size below 300 nm [30]. Above 300 nm, a significant proportion of the silica particles remain trapped in the lungs and the liver [31].

The emulsion process to synthesize microparticles was slightly adjusted to produce the particles in the nanometer range. From a process point of view, the main difference between the two processes (see Figs. 2 and 3) is the order of addition of the different chemicals. This results in the formation of an emulsion prior to addition of the silicon precursor in the case of the nanoparticles, rather than gelation and emulsification occurring at the same time, as in the microparticle synthesis. In other words, the process in Fig. 2 can be viewed as an emulsification (and rapid gelation) of a sol–gel solution whereas the process in Fig. 3 can be viewed as the gradual gelation of a stable micro-emulsion. In the latter case, the silicon alkoxide is introduced in the oil phase and slowly diffuses through the surfactant wall in the water droplets where it is hydrolysed and condensed [32]. In respect to the emulsion properties, surfactants with HLB less than 10 are preferred for microsphere synthesis (such as Span 80 (HLB 4.3) and

Span 20 (HLB 8.6)), whereas surfactants with mid-range HLB (between 10 and 15) are normally selected for nanoparticle synthesis (NP-5: 10, NP-9: 13, Triton X-114: 12.4, and AOT (10–15)).

5.2 Control of the size

As for the synthesis of microspheres, the nanoparticle size depends on the initial emulsion droplet size and thus on chemical parameters such as the nature of the surfactant–solvent couple and the water to surfactant mole ratio.

Figure 18 shows the dramatic influence of the nature of the surfactant–solvent couple on the particle size. In the case of the NP-9/cyclohexane emulsion synthesis, very small water pools (typically around 5 nm [31]) of the stable micro-emulsion are further stabilised by the presence of a co-surfactant, 1-pentanol. In contrast, although the Triton X-114/toluene forms an emulsion, the opacity of the emulsion, resulting from the light scattering by the water pools in the solvent, suggests a larger droplet size around 100 nm. This difference in the initial emulsion droplet size leads to the synthesis of particles with two drastically different size distributions (see Fig. 18b).

The size of the particles can be further tuned by adjusting emulsion parameters such as the water to surfactant ratio and the overall amount of alkoxide introduced in the system. The water to surfactant mole ratio determines the size of the water pool as well as the amount of free water (as opposed to bound water which is used for solvating the surfactant polar head, and trapped water which is associated with hydrophilic part of the surfactant), which can participate in the hydrolysis of the alkoxide and thus the particle synthesis [33]. In general, the higher the water to surfactant ratio, the bigger the water pools thus the bigger the particles. The overall amount of precursor introduced in the system also influences the particle size (see Fig. 19). For a fixed water to surfactant ratio, which translates into a fixed number of water pools or in term of nucleation and growth, into a fixed number of nucleation centres, increasing the amount of TMOS increases the amount of monomer available for growth and thus the average particle size. It is important to note, as discussed in detail in [32], that the synthesis of nano-particles in basic environment deviates slightly from the micro-reactor analogy in the fact that it does involve some additional growth by scavenging of the contents of other water pools. This process, which takes place during the aging step, is especially important in the case of the synthesis in NP-9 emulsion where slow hydrolysis of TEOS requires long synthesis times.

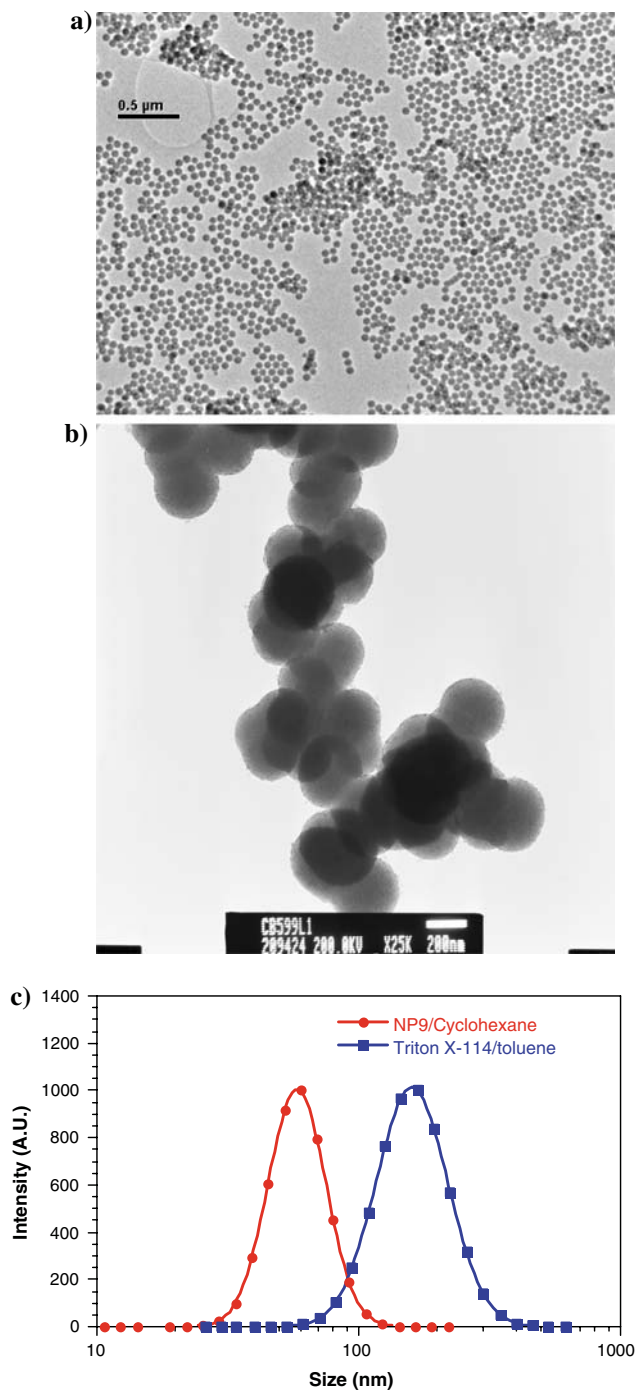


Fig. 18 Influence of the nature of the surfactant and solvent on the nanoparticles morphology (a) TEM of particle synthesised with NP9 in cyclohexane, (b) triton X-114 in Toluene and (b) corresponding size distribution measured by PCS

5.3 Control of release

More importantly, the difference observed in the internal structure of microparticles synthesised in acid and base, is preserved in the nanoparticles. Acid catalysis gives rise to a

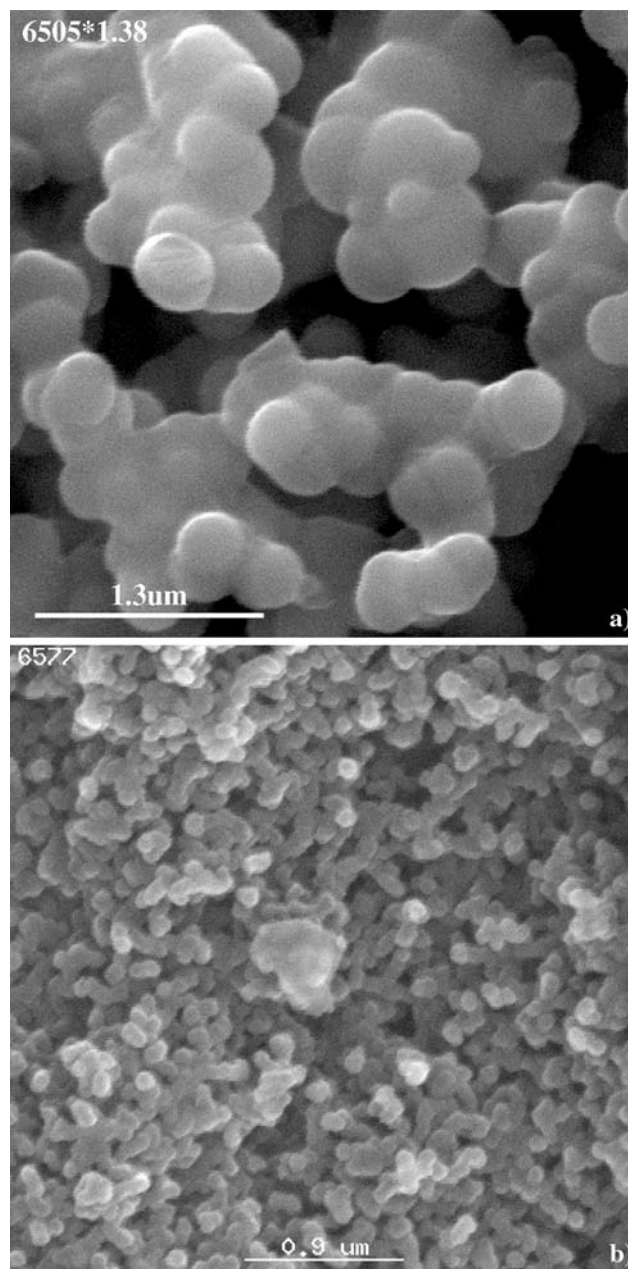


Fig. 19 Influence of the water to surfactant molar ratio on the particles synthesised with Triton X-114 with a water surfactant ratio of 16 with (a) alkoxide/surfactant = 0.5 and (b) alkoxide/surfactant = 0.1

microporous structure with high surface area, while basic catalysis produces nanoparticles with mesoporous or fully dense structures depending on the pH [25].

The potential to produce dense spheres at very high pH has been used to fully encapsulate (i.e. without leaching) organo-metallic dyes and radiolabels. This process was used to radiolabel our nanoparticles with ⁶⁷Ga complexes for in vivo biodistribution studies. Large pore sizes (i.e. mesoporosity) leads to fast diffusion of the active out of the

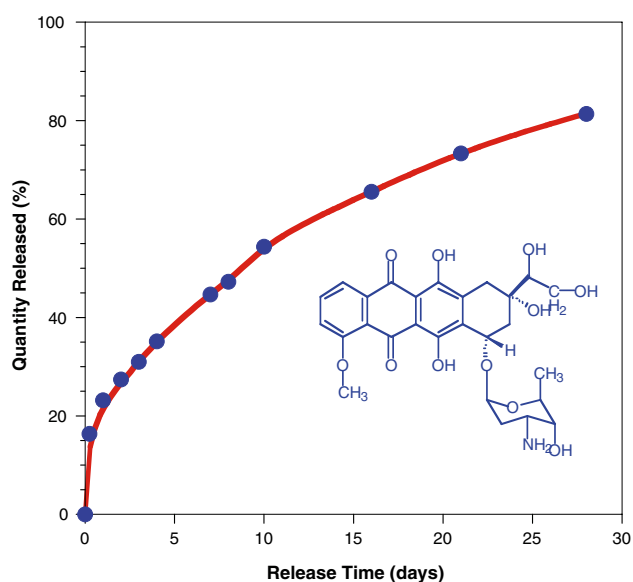


Fig. 20 Release curves of doxorubicin from 30 nm nanoparticles synthesised at pH = 1

particles. This, combined with the small distance that the active has to travel in nanoparticles, leads to instant “burst” release. In contrast, acid catalysed nanoparticles release their payload in controlled fashion as shown in Fig. 20 where doxorubicin, a classical anti-tumour agent is released over several weeks.

5.4 Control of the aggregation

One of the main reasons precluding a wider use of nanoparticles is their high propensity to aggregate and flocculate. In the case of porous particles, storage in liquid form would lead to a gradual release of the active from the nanoparticles. It was therefore imperative to design a method for storing the nanoparticles in a dry state while preventing physical and irreversible aggregation.

This was achieved by freeze-drying the nanoparticle suspension in a concentrated solution of water-soluble salt (e.g. NaCl). The freeze-dried particles (see Fig. 21) are encased in a gangue of salt which prevents them from physically touching one another. This solid formulation can be stored safely in the dry state for months. When needed, the particles can be easily redispersed by adding water to the freeze-dried powder under gentle sonication.

5.5 Conclusion

Both the size of the nanoparticles and their release characteristics can be controlled precisely by controlling the emulsion and sol-gel chemical parameters. The particle size is controlled by the emulsion parameters such as the nature of the surfactant and solvent, as well as the water to

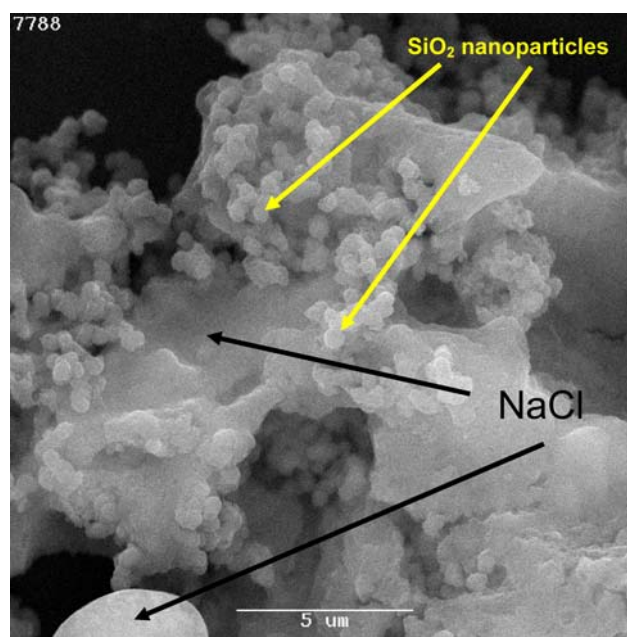


Fig. 21 SEM micrograph of re-dispersible freeze dried nanoparticles

surfactant ratio and the alkoxide to water ratio. The release rate of the particles can be independently tailored by controlling the internal porous structure of the particles. This can be achieved, for example, by controlling the pH of the water pools, and thus orienting the sol-gel network formation towards micro, meso or non-porous particles. It is important to note that because of the smaller diffusion length (nanometer versus microns), the degree of control of the release in nanoparticles is lower than that achieved in microparticles.

6 Conclusions

The release rate of small molecules encapsulated in sol-gel matrices can be precisely tailored by controlling the internal microstructure of the resulting gel. By controlling the pore size one can restrict the diffusion of the active molecules out of the gel. Denser microporous gel will provide slow and extended release, whereas mesoporous gel will provide faster release. The introduction of organically modified silica can also decrease the release rate by increasing the hydrophobicity of the matrix and thus slowing the penetration of water inside the small pores. This ability to control the release rate of encapsulated molecules can be extended from xerogel monoliths to silica microspheres by performing the sol-gel polymerisation inside the polar droplets of a “water”-in-oil emulsion. The particle size can be tailored by controlling the emulsion parameters such as the nature of the solvent and surfactant.

The release trends observed in the xerogels are preserved in the microparticles, confirming the validity of the micro-reactor approach, which allows for independent control of the size and internal structure of the sphere. This approach can be further extended to nanoparticles, by using stable micro-emulsions with nanometer size droplets. Both the size of the nanoparticles and their release characteristics can still be precisely controlled by the emulsion and sol-gel chemical parameters. This shows that the efficient compartmentalization offered by the O/W emulsion, allows the sol-gel reactions to proceed almost unaltered on the nano-scale.

Although in the present paper this concept is limited to the encapsulation of small hydrophilic molecules due to the requirement of the active to be preferentially soluble in the polar droplets, it has been recently expanded to the encapsulation of larger bio-molecules [34] using aqueous colloidal silica as sol-gel precursors and the encapsulation of hydrophobes using double emulsions or oil-in-water emulsions [35] This versatility, combined with protection of the active offered by the silica matrix and the ability to independently tailor particle size and release rate, makes this technology very attractive for delivery applications in the food, homecare, chemical, biocide, pesticide, cosmetic and pharmaceutical markets.

Acknowledgements We would like to thank our colleagues from ANSTO with various sample characterizations in particular Joel Davis and Dr. Arthur Day for SEM and Dr. Greg Lumpkin for TEM on the Triton X-114 samples.

References

- Zink JI, Dunn BS (1991) *J Mater Chem* 1(6):903
- Boettcher H, Kallies K-H, Haufe H, Seidel J (1999) *Adv Mater* 11(2):138
- (a) Braun S, Rappoport S, Zusman R, Avnir D, Ottolenghi M (1990) *Mater Lett* 10:1; (b) Avnir D, Braun S, Ottolenghi M (1992) *ACS Symp Ser* 499:384; (c) Avnir D, Braun S, Lev O, Ottolenghi M (1994) *Chem Mater* 6:1605; (d) Dave BC, Dunn B, Valentine JS, Zink JI (1996) 622:351; (e) Wie Y, Xu J, Feng Q, Dong H, Lin M (2000) *Mater Lett* 44:6
- (a) Gill I, Ballesteros A (1998) *JACS* 120:8587; (b) Livage J, Roux C, Da Costa J-M, Desportes I, Quinson J-F (1996) *J Sol-Gel Sci Technol* 7:45; (c) Rietti-Stait M, Ronen D, Mandelbaum RT (1996) *J Sol-Gel Sci Technol* 7:77; (d) Finnie KS, Bartlett JR, Woolfrey JL (2000) *J Mater Chem* 10:1099
- (a) Dire S, Cavazza A, Campostrini R, Carturan G (1992) *Eur Mater Res Sci Monogr* 5:151; (b) Boninsegna S, Bosetti P, Carturan G, Dellagiacomma G, Dal Monte R, Rossi M (2003) *J Biotechnol* 100(3):277
- Brinker CJ, Scherer GW (1990) *Sol-gel science: the physics and chemistry of sol-gel processing*. Academic Press, San Diego
- Barbé C, Bartlett J, Kong L, Finnie K, Lin HQ, Larkin M, Calleja S, Bush A, Calleja G (2004) *Adv Mater* 16:1959
- Radin S, Ducheyne P, Kamplain T, Tan BH (2001) *J Biomedical Res* 57:313
- Ahola M, Sailyloja ES, Raitavuo MH, Vaahtio MM, Salonen JI, Yli-Urpo AUO (2001) *Biomaterials* 22:2163; Roveri N, Morpurgo M, Palazzo B, Parma B, Vivi L (2005) *Anal Bioanal Chem* 381:601
- Kortesuo P, Ahola M, Kangas M, Yli-Urpo TA, Kiesvaara J, Marvola M (2001) *Int J Pharm* 221:107
- Bottcher H, Slowik P, Suss W (1998) *J Sol-gel Sci Technol* 13:277
- Santos EM, Radin S, Ducheyne P (1999) *Biomaterials* 20:1695
- (a) Siemenska L, Ferguson M, Zerda TW, Couch E (1997) *J Sol-Gel Sci Technol* 8:1105; (b) Viitala R, Jokinen M, Liisa Maunu S, Jalonen H, Rosenholm JB (2005) *J Non-Crystal Sol* 351:3225
- Ahola M, Kortesuo P, Kangasniemi I, Kiesvaara TJ, Yli-Urpo A (2000) *Int J Pharm* 195:219
- Lopez T, Manjarrez J, Rembao D, Vinogradova E, Moreno A, Gonzalez RD (2006) *Mater Lett* 60:2903
- Lopez T, Sotelo J, Navarrete J, Ascencio JA (2006) *Opt Mater* 29:88
- Koskinen MK, Toriserva M, Ahonen M, Kahari V-M, Salonen J (2003) *Controlled release society 30th annual meeting proceedings 2003*, 597
- Kortesuo P, Ahola M (1997) *PCT WO* 97/45367
- Kortesuo P, Ahola M, Kangas M, Jokinen M, Leino T, Vuorilehto L, Laakso S, Kiesvaara AJ, Yli-Urpo A, Marvola M (2002) *Biomaterials* 23:2795
- Czuryszkiewicz T, Areva S, Honkanen M, Lindén M (2005) *Coll Surfaces A* 254:69
- Barbe CJ, Bartlett JR (2001) *PCT WO* PCT WO 01/62232
- Finnie KS, Waller DJ, Perret FL, Krause-Heuer AM, Lin HQ, Hanna JV, Barbé CJ submitted to *J Mater Sci: Materials in Medicine*
- Brinker CJ, Scherer GW (1990) *Sol-gel science: the physics and chemistry of sol-gel processing*. Academic Press, San Diego, pp 212–213
- Atanacio AJ, Latella BA, Barbe CJ, Swain MV (2005) *Surf Coat* 192:354–364
- Brinker CJ, Scherer GW (1990) *Sol-gel science: the physics and chemistry of sol-gel processing*. Academic Press, San Diego, pp 467–468
- Bush A, Beyer R, Trautman R, Barbe C, Bartlett J (2004) *J Sol-Gel Sci Technol* 32:85
- Arriagada FJ, Osseo-Asare K (1999) *J Coll Interface Sci* 211:210
- Chang C-L, Fogler HS (1997) *Langmuir* 13:3295
- Arriagada J, Osseo-Asare K (1994) *J Dispersion Sci Technol* 15(1):59–71
- (a) Jain R (1998) *J Control Release* 53:49; (b) Moghimi SM, Hunter AC, Murray JC (2001) *Pharmaco Rev* 53:283; (c) Carmeliet P, Jain RK (2000) *Nature* 407:249
- Borchardt G, Brandriss S, Kreuter J, Margel S (1994) *J Drug Targeting* 2:61
- Finnie K, Bartlett J, Barbe C, Kong L (2007) *Langmuir* 23:3017
- Osseo-Asare K (1999) *Microemulsion-mediated synthesis of nanosize oxide materials*. Handbook of microemulsion science and technology. Marcel Dekker, pp 549–603
- Finnie KS, Jacques DA, McGann MJ, Blackford MG, Barbé CJ (2006) *J Mater Chem* 46:4494
- Barbé CJ, Finnie KS, Kong L (2007) *CRS Newsl* 24(2):17